Inorganic Chemistry
Article

Inorg. Chem. **2010**, *49*, 1503–1509 **1503**
DOI: 10.1021/ic901771x

$K_{23}Au_{12}Sn_9$—An Intermetallic Compound Containing a Large Gold−Tin Cluster: Synthesis, Structure, and Bonding

Bin Li, Sung-Jin Kim, Gordon J. Miller, and John D. Corbett*

Ames Laboratory−DOE and Department of Chemistry, Iowa State University, Ames, Iowa 50011

Received September 4, 2009

A polyanionic unit $\{Au_{12}Sn_9\}$ with a novel "corrugated sheet" shape occurs in $K_{23}Au_{12}Sn_9$. The compound was obtained by fusion of the pure elements in tantalum ampules at high temperatures followed by programmed cooling, and the structure was determined by X-ray diffraction: $I\bar{4}2m$ (No. 121), a = 20.834(3), c = 6.818(1) Å, Z = 2. The large heteroatomic cluster has D_{2d} point symmetry and features a central four bonded (4*b*-) Sn, eight 3*b*- or 2*b*-Sn on the perimeter, and 24 linking nearly linear Sn−Au bonds at 12 Au atoms. Formula splitting according to the *Zintl* concept suggests that the compound is one electron deficient, and linear muffin-tin-orbital (LMTO) electronic structure calculations show that the Fermi level (E_F) lies near a band gap at around 0.5 eV, that is, an incompletely filled valence band in concert with favorable atom packing. Large relative −ICOHP values for Au−Sn are consistent with the observed maximization of the number of heteroatomic bonds, whereas the numerous K-Sn and K-Au contacts contribute ∼40 % of the total -ICOHP. Extended-Hückel population and molecular orbital analyses indicate that the open band feature originates from 5p states that are associated with the 2*b*-corner Sn atoms. In accord with the electronic structure calculations, magnetic susceptibility measurements show a nearly temperature-independent paramagnetic property.

1. Introduction

Larger anionic metal clusters are of wide interest because they may feature novel bonding/electronic requirements in closed systems, but these may also serve as suitable building units for higher dimensional systems that exhibit beautiful (symmetrical) shapes.[1] Such discrete clusters are common in alkali-metal/tetrel systems (tetrel (*Tt*) = Si−Pb) and exhibit a rich derivative chemistry (such as ligand functionalization, oxidative couplings, controlled decomposition).[2−4] The majority of homoatomic *Tt* clusters are convex polyhedra that have special valence electron requirements (Wade's rules, aromaticity).[5−8] On the other hand, non-spherical homoatomic anionic clusters (of more than three atoms) mainly consist of smaller metal chains (up to eight atoms), star-shaped, or planar square units.[9] In the heteroatomic cases, centered tetrahedra (e.g., $\{SnSb_4\}^{8-}$),[10] edge/vertex sharing tetrahedra (e.g., $\{Sn_2Bi_6\}$[10,11]), ethane-like (e.g., $\{Sn_2Te_6\}^{6-12}$), CO_3^{2-}-like (e.g., $\{AgSn_3\}$[11−13]), or simple triatomic clusters (e.g., $\{ZnSn_2\}^{6-14}$) have been reported. Generally, synthesis of larger units, especially with electron-poor elements, is hampered by a tendency to form networks In that respect gold-rich clusters have not been reported so far.

Fruitful and traditional routes to such clusters are reactions between active- and post-transition metals.[15] In extreme (intermetallic) cases large electronegativity (*EN*) differences between the components allow bond optimization and closed-shell (poly)anionic *Zintl* phases to form.[16] Their structures can often be tuned through thoughtful choices of the components and their stoichiometry (and luck!). Although electronic factors, such as octet or Wade's rules may be decisive in these systems, such "optimal" scenarios are often dictated by other energy terms, such as packing efficiency in a "good" structure. The unexpected but frequent cases with open-band (open-shell) electronic structures are

*To whom correspondence should be addressed. E-mail: jcorbett@iastate.edu.

(1) Müller, A. *Science* **2003**, *300*, 749.
(2) Fässler, T. F. *Coord. Chem. Rev.* **2001**, *215*, 347.
(3) Sevov, S. C.; Goicoechea, J. M. *Organometallics* **2006**, *25*, 5678.
(4) Guloy, A.; Ramlau, R.; Tang, Z.; Schnelle, W.; Baitinger, M.; Grin, Y. *Nature* **2006**, *443*, 320.
(5) Corbett, J. D. *Inorg. Chem.* **2000**, *39*, 5178.
(6) Corbett, J. D. *J. Chem. Soc., Dalton Trans.* **1996**, 575.
(7) Fässler, T. F.; Hoffmann, S. D. *Angew. Chem.* **2004**, *116*, 6400.
(8) Chen, Z.; Neukermans, S.; Wang, X.; Janssens, E.; Zhou, Z.; Silverans, R. E.; King, R. B.; v. Ragué Schleyer, P.; Lievens, P. *J. Am. Chem. Soc.* **2006**, *128*, 12829.
(9) v. Schnering, H. G. *Angew. Chem.* **1981**, *93*, 44.
(10) Eisenmann, B.; Klein, J. *Z. Naturforsch.* **1988**, *43B*, 1156.
(11) Xia, S. Q.; Bobev, S. *Inorg. Chem.* **2008**, *47*, 1919.
(12) Dittmar, G. *Z. Anorg. Allg. Chem.* **1979**, *453*, 68.
(13) Lupu, C.; Downie, C.; Guloy, A. M.; Mao, J. G. *J. Am. Chem. Soc.* **2004**, *126*, 4386.
(14) Kim, S.-J.; Kraus, F.; Fässler, T. F. *J. Am. Chem. Soc.* **2009**, *131*, 1469.
(15) Corbett, J. D. *Chem. Rev* **1985**, *85*, 383.
(16) (a) Zintl, E.; Dullenkopf, W. *Z. Phys. Chem.* **1932**, *B 16*, 195. (b) *Chemistry, Structure and Bonding of Zintl Phases and Ions*; Kauzlarich, S., Ed; VCH Publishers: New York, 1996. (c) Schäfer, H.; Eisenmann, B.; Müller, V. *Angew. Chem., Int. Ed.* **1973**, *12*, 683.

Published on Web 01/11/2010

often referred to as metallic salts or metallic *Zintl* phases[17] because they still retain some physical attributes, such as brittleness, solubility, and stoichiometric compositions. However, bonding requirements may be accommodated with an excess or shortage of valence electrons which lead to open bands and metallic conductivity. These may be understood as borderline compounds between *Zintl* (closed-band) and typical polar intermetallic phases.

Within this context we have focused on more-or-less gold-rich polyanionic intermetallic systems and in the discovery of new bonding motifs. The known combinations of active, gold, and *Tt* metals in this phase region mainly occur in three-dimensional (3D) systems, such as for KAu_4Sn_6 and KAu_3Sn_3 with condensed $[Au_{10}Sn_{10}]$ polyhedra,[18] and $K_{12}Au_{21}Sn_4$,[19a] $A_4Au_7Tt_2$ (A = K, Cs; Tt = Ge, Sn),[20] K_3Au_5Pb[21] with networks based on Au_4 tetrahedra. Unusual features to date often seem to occur in compositions with such relatively large proportions of Au plus large or small proportions of alkali metal atoms in compounds with either triel or tetrels components. Here, we report about $K_{23}Au_{12}Sn_9$, a novel phase that contains a unique heteroatomic cluster.

2. Experimental Section

Synthesis. All reactants and products were manipulated in the dry N_2 atmosphere (H_2O level <0.1 ppm) of a glovebox. The synthesis succeeded by direct fusion of stoichiometric amounts of the high purity elements: K: 99.9% (Alfa-Aesar); Au: 99.997% (Ames Lab); Sn: 99.99% (Alfa-Aesar), followed by a cooling routine. The elements were sealed within 9 mm diameter Ta containers that were, in turn, enclosed in evacuated and well-baked silica jackets to protect the former from air. The temperature treatment included heating up to 650 °C (120 deg/h), holding for 4 h, cooling to 350 °C (6 deg/h), and equilibration for 160 h. A later reaction starting with composition of the refined structure gave high yields of the product (>90% on the basis of powder pattern data). The brittle compound shows dark metallic luster and rapidly decomposes in moist air. Attempts to prepare the Na and Rb analogues or a Na-doped electron precise "$K_{23}NaAu_{12}Sn_9$" were unsuccessful. To obtain diamagnetic compounds, reactions with adjusted electron counts, $K_{22}AeAu_{12}Sn_9$ (Ae = Ca, Sr), were also carried out. Evaluation of EDX and X-ray diffraction data gave no hint for the formation of the quaternary phase, rather Ca in these experiments formed unknown byproducts.

EDX analyses of different crystallites were accomplished on a JEOL 5910LV electron microscope and a Noran-Vantage detector operating at 20 kV acceleration voltage. The average composition (at %) is in good agreement with the crystallographically refined composition, respectively: K 53.3(5) [52.3]; Au 27.2(9) [27.3], Sn 19.5(7) [20.5]. In addition to $K_{23}Au_{12}Sn_9$ an unknown K-poorer and Au-richer byproduct was also detected.

X-ray Studies. Powder diffraction data were collected with a Huber 670 Guinier powder camera equipped with an area detector and Cu Kα radiation (λ = 1.540598 Å). Finely ground samples were homogeneously dispersed in the glovebox between two Mylar sheets with the aid of a little vacuum grease. These were in turn held between a split aluminum ring that provided airtight seals. Unit cell parameters were refined with the WinX-Pow program[22] and used for calculations with single crystal structural data. The powder results from a stoichiometric synthesis showed that $K_{23}Au_{12}Sn_9$ forms as the majority component (>90 vol %) accompanied with few weak unindexed reflections, Supporting Information, Figure S1.

Single crystal diffraction data sets were collected at 293(2) K with the aid of Mo Kα radiation and a Bruker Apex I diffractometer. The data came from a set of 606 frames with 0.3° scans in ω and exposure times of 10 s per frame. Reflection intensities were integrated with the SAINT subprogram in the SMART software package,[23a] and space group determination was done with the aid of XPREP in the SHELXTL 6.1 software package.[23b] After an empirical absorption correction,[24] the structure was solved by direct methods with the aid of SHELXTL 6.1 and subsequently refined anisotropically in the indicated noncentrosymmetric space group $I\bar{4}2m$ by full-matrix least-squares on F_o^2, ultimately with a secondary extinction parameter. Two Sn, three Au, and five K positions could be unambiguously assigned. K5 shows a large anisotropic displacement parameter (ADP) along c, as was also observed in the Fourier electron density map contoured in a plane that included K5 and Sn3, Supporting Information, Figure S2, a feature that is ascribed to its tunnel-like environment in that direction (below). Freeing its occupancy factor led to 98(3) % occupancy and almost unchanged ADPs. The Flack parameter[25] of 0.01(2) indicated the correct absolute structure had been solved. Some data collection and refinement parameters are collected in Table 1, and the atomic positions and isotropic equivalent displacement

Table 1. Selected Crystal and Refinement Data for $K_{23}Au_{12}Sn_9$

empirical formula	$K_{23}Au_{12}Sn_9$
fw/g·mol^{-1}	4331.11
space group, Z	$I\bar{4}2m$ (No. 121), 2
unit cell parameters	a, b = 20.834(3) Å
	c = 6.818(1) Å
	V = 2959.5(8) Å^3
ρ_{calcd}/g·cm^{-3}	4.86
μ/mm^{-1} (Mo Kα)	34.95
data/restraints/para.	1870/0/57
R_1/wR_2 [$I > 2\sigma(I)$]	0.037/0.094
R_1/wR_2 (all data)	0.050/0.115
absolute structure parameter	0.01(2)

Table 2. Atomic Coordinates and Equivalent Isotropic Displacement Parameters (Å^2 × 10^3) for $K_{23}Au_{12}Sn_9$

atom	Wyck.	x	y	z	U_{eq}
Au1	8*i*	0.5825(1)	0.5825(1)	0.8211(2)	37(1)
Au2	16*j*	0.7507(1)	0.5911(1)	0.8501(1)	40(1)
Sn1	2*b*	1/2	1/2	0	29(1)
Sn2	8*i*	0.6642(1)	0.6642(1)	0.6502(2)	36(1)
Sn3	8*g*	0.8287(1)	1/2	0	41(1)
K1	16*j*	0.6714(2)	0.4578(2)	0.7517(6)	45(1)
K2	16*j*	0.8410(2)	0.5981(2)	0.4621(6)	51(1)
K3	2*a*	1/2	1/2	1/2	47(3)
K4	8*i*	0.7176(2)	0.7176(2)	0.1443(9)	43(1)
K5[a]	4*d*	0	1/2	1/4	271(20)

[a] The occupancy at K5 can be refined to 0.98(3) which hardly changes its displacement parameters.

(17) Nesper, R. *Angew. Chem., Int. Ed.* **1991**, *30*, 189.
(18) Li, B.; Corbett, J. D. *Inorg. Chem.* **2008**, *47*, 3610.
(19) (a) Li, B.; Kim, S.-J.; Miller, G. J.; Corbett, J. D. *Inorg. Chem.* **2009**, *48*, ASAP; (b) Kim, S.-J.; Miller, G. J.; Corbett, J. D. *Z. Anorg. Allg. Chem.* **2010**, *636*, 67.
(20) (a) Sinnen, H.-D.; Schuster, H.-U. *Z. Naturforsch.* **1981**, *36b*, 833. (b) Zachwieja, U.; Wlodarski, J. *Z. Anorg. Allg. Chem.* **1998**, *624*, 1443. (c) Zachwieja, U.; Wlodarski, J. *Z. Anorg. Allg. Chem.* **1995**, *621*, 975.
(21) Zachwieja, U.; Wlodarski, J. *Z. Anorg. Allg. Chem.* **1998**, *624*, 1569.
(22) *WinXPow*, 2.10; STOE & Cie GmbH: Darmstadt, Germany, 2004.
(23) (a) *SMART*; Bruker AXS, Inc.: Madison, WI, 1996. (b) *SHELXTL*; Bruker AXS, Inc.: Madison, WI, 1998.
(24) (a) *X-Red: Stoe Data Reduction Program*, Vers. 1.22; Stoe & Cie GmbH: Darmstadt, Germany, 2001. (b) *X-Shape: Crystal Optimization for Numerical Absorption Correction*, Vers. 1.06; Stoe & Cie GmbH: Darmstadt, Germany, 1999.
(25) Flack, H. D. *Acta Crystallogr., Sect. A* **1983**, *39*, 876.

Table 3. Selected Bond Lengths [Å], Their Number (n) per Unit Cell ($Z = 2$), −ICOHP Values[a], and Percentiles for $K_{23}Au_{12}Sn_9$[b]

atom pair	n	distance	−ICOHP (/bond·mol)	−ICOHP (/cell)	−ICOHP (%)
Au1−Sn1	8	2.720(1)	2.63	126.6 (all Au−Sn)	60
Au1−Sn2	8	2.673(2)	2.62		
Au2−Sn2	16	2.725(1)	2.52		
Au2−Sn3	16	2.699(1)	2.77		
K−Au	120	3.23−3.55	av 0.31	37.2	19
K−Sn	108	3.41−3.96	av 0.41	44.2	21

[a] Per bond and per cell [eV]. [b] Distance Cutoff is set to 4 Å.

parameters are given in Table 2. Important bond distances are listed in Table 3, and the cif output is provided in the Supporting Information.

Electronic Structure Calculations. Tight-binding electronic structure calculations were performed according to the linear muffin-tin-orbital (LMTO) method in the atomic sphere approximation (ASA).[26] For space filling within the ASA, eight interstitial (empty) spherical (ES) sites were necessary to avoid too large overlaps of the atom-centered spheres. The positions and radii of the atomic and empty spheres were calculated automatically so that the superposition of the spherical potentials approximated the full potential as well as possible,[27] with overlaps limited to 18% between atom-centered spheres, 19% between atomic and interstitial sites, and 20% between any two interstitial spheres. The radii of the spheres [Å] were K: 1.97−2.29; Au: 1.53−1.54; Sn: 1.62−1.67; ES: 0.79−0.93, and the basis set consisted of K 4s/(4p)/3d, Au 6s/6p/5d/(5f), Sn 5s/5p/(5d/4f), with downfolded[28] orbitals in parentheses. Reciprocal space integration was performed on a grid of 262 irreducible k-points. For bonding analysis, the energy contributions of all electronic states for selected bond types were evaluated from COHP curves.[29] Integration over all filled states gave −ICOHP values which are energy correlated overlap populations. The COHP diagrams are drawn by reversing their values (−COHP vs E), so that the values are positive for bonding interactions. Molecular orbital and Mulliken population analyses for the $\{Au_{12}Sn_9\}$ cluster unit were made with the aid of extended-Hückel-TB calculations (EHTB) and the CAESAR2 program.[30] A weighted H_{ij} formula was used and the following Coulomb integrals (H_{ii} /eV) and orbital exponents (ζ) were employed:[31] Au 6s: −10.92/2.60, Au 6p: −5.55/2.58, Au 5d: −15.08/6.16 (2.79), Sn 5s: −16.16/2.12, Sn 5p: −8.32/1.82. To assess the atom coloring, calculations on a $\{In_{12}In_9\}^{23-}$ cluster were done with In 5s: −12.60/1.90, In 5p: −6.19/1.68.[31]

Magnetic Measurements. The magnetization of $K_{23}Au_{12}Sn_9$, Supporting Information, Figure S6, was measured on a Quantum Design MPMS SQUID magnetometer at a field of 1 T over 6−300K. A sample of 62 mg was sealed within a fused silica tube in which it was held between two tightly fitting rods of the same material.

3. Results and Discussion

Crystal Structure of $K_{23}Au_{12}Sn_9$. The compound crystallizes in the noncentrosymmetric space group $I\bar{4}2m$ with the Pearson code $tI88$. The [001] projection of the unit cell, Figure 1a, shows 12 Au (yellow) and 9 Sn (blue) atoms in a large open cluster that is immersed in a matrix of K atoms (red). The ∼[110] view, Figure 1b, emphasizes their strongly folded sheet-like shape. Next nearest intercluster Sn−Sn, Au−Sn, and Au−Au distances are > 5.7 Å.

These striking 21-member {AuSn} clusters are centered by Sn1 atoms at (0, 0, 1/2) and (1/2, 1/2, 0), and are distributed within the cell according to a $\bar{4}$ axis along (0, 0, z). A stereograph, an inset in Figure 2a, shows their D_{2d} point symmetry with the normal C_2 axis along [001] and through Sn1. Therefore, the cluster can be generated by means of two mirror planes (both along the Sn1−Sn2 vectors) or by the condensation of an eight-membered ring, [Sn1Au1Sn2Au2Sn3Au2Sn2Au1] puckered by ± 2.39 Å, Figure 2b. (From a remote point of view, this novel unit may also be regarded as four circles of alternating Au and Sn atoms around the central Sn1, Figure 2a).

Appropriate to their p-valent character, all Sn atoms show roughly tetrahedral coordination (when imagined lone pairs are included for closed shell octets), with bond angles ranging from 81° (at Sn2) to 106° at Sn3. The hypothetical tetrahedron around Sn1 is compressed along c with 102−127° bond angles. On the other hand, the two (largely s-valent) Au atoms are quasi linear coordinated with angles 169° at Au2 and 179° at Au1. Gold in linear coordination with heteroatoms is commonly observed for cationic Au(I) species but has also been reported in *zigzag* anionic chains of alternating atoms with terminal pnictogen[19b,32] or chalcogen[33] atoms.

Au−Sn bond distances range from 2.67−2.73 Å, only slightly longer than the 2.64 Å sum of single bond covalent radii derived from very different homoatomic and neutral molecular environments (Au: 1.24; Sn: 1.40 Å)[34] and are close to those in the *Zintl* phase K_3AuSn_4, 2.77 Å.[35] Considering formal charges, it is noteworthy that Au−Sn distances are rather uniform and not significantly longer at the boundary 2*b*-$Sn3^{2-}$ or shorter at the $Sn1^0$ atoms. Another feature is the presence of only heteroatomic contacts (24 Au−Sn bonds) with the Au atoms at the less bonded positions, which may be explained by the preference of more electronegative elements on sites with higher electron densities (below)[36] as

(26) Krier, G.; Jepsen, O.; Burkhardt, A.; Andersen, O. K. *TB-LMTO-ASA Program*, Vers. 4.7; Max-Planck-Institut für Festkörperforschung: Stuttgart, Germany, 1995.
(27) Jepsen, O.; Andersen, O. K. *Z. Phys. B* **1995**, *97*, 35.
(28) (a) Lambrecht, W. R. L.; Andersen, O. K. *Phys. Rev. B* **1986**, *34*, 2439. (b) Löwdin, P. *J. Chem. Phys.* **1951**, *19*, 1396.
(29) Dronskowski, R.; Blöchl, P. E. *J. Phys. Chem.* **1993**, *97*, 8617.
(30) Ren, J.; Liang, W.; Whangbo, M.-H. *CAESAR2 for Windows*; Prime-Color Software, Inc., North Carolina State University: Raleigh, NC, 1998.
(31) Alvarez, S. *Tables of Parameters for Extended Hückel Calculations*; Departamento de Quimica Inorganica, Universitat de Barcelona: Barcelona, Spain, 1987.
(32) Mues, C.; Schuster, H. U. *Z. Naturforsch.* **1980**, *35*, 1055.
(33) Bronger, W.; Kathage, H. U.; Sauer, C. *J. Alloys Compd.* **1992**, *187*, 351.
(34) Pyykkö, P.; Atsumi, M. *Chem.—Eur. J.* **2009**, *15*, 186.
(35) (a) Zachwieja, U.; Wlodarski, J. *Z. Anorg. Allg. Chem.* **2004**, *630*, 993. (b) Zachwieja, U.; Müller, J.; Wlodarski, J. *Z. Anorg. Allg. Chem.* **1998**, *624*, 853.
(36) (a) Miller, G. J. *Eur. J. Inorg. Chem.* **1998**, 523. (b) Nordell, K. J.; Miller, G. J. *Angew. Chem., Int. Ed. Engl.* **1997**, *36*, 2008. (c) Nordell, K. J.; Miller, G. J. *Inorg. Chem.* **1999**, *38*, 579.

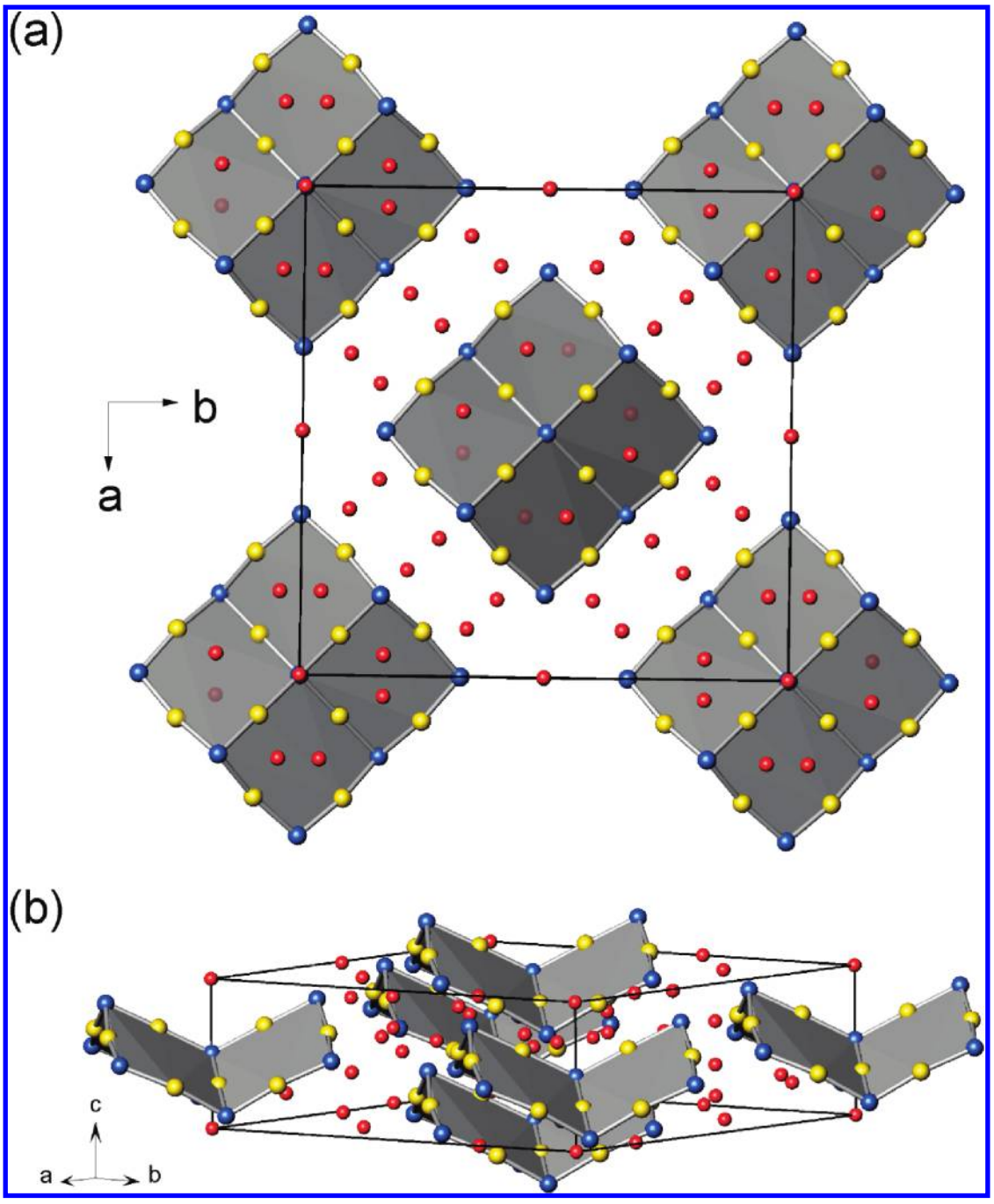

Figure 1. Perspective views of the unit cell of $K_{23}Au_{12}Sn_9$ along (a) [001] and (b) ~[110]. The gray $\{Au_{12}Sn_9\}$ units are emphasized and Sn, Au, and K atoms are drawn as blue, yellow, and red spheres, respectively.

well as by evidently stronger heteroatomic bonding in situations of this type.[18,19]

The clusters are surrounded and well separated from each other by a cage of 62 K atoms (< 4 Å), Supporting Information, Figure S3. The K−Au and K−Sn distances range from 3.23−3.55 Å and 3.41−3.96 Å, respectively, Table 3. The coordination of the Au and Sn atoms by the cations, Figure 2b, seems to play an important role; especially noteworthy are the eight K neighbors around the (more open) corner Sn3 atoms (purple lines). A further point of notice is the less restrictive environment of K5, which is located in tunnel-like voids that furnish only four longer K−Sn separations at 3.956(2) Å and allow large anisotropic displacements along *c*. We have earlier reported similar entrapments and significant cation displacements in open Au−In tunnel networks.[37] Coordination figures around the K atoms in the Supporting Information, Figure S4, show K1−K4 atoms with 2−4 Au and 2−3 Sn neighbors, whereas the less well localized K5 (Supporting Information, Figure S2) only has four longer contacts to Sn3.

Electronic Structure and Bonding. Although many binary intermetallic *A*-Sn compounds satisfy the *Zintl* concept; that is, their structures can be rationalized by applying octet rules, the presence of transition metals often requires more detailed bonding analyses. With

(37) Li, B.; Corbett, J. D. *Inorg. Chem.* **2007**, *46*, 6022.

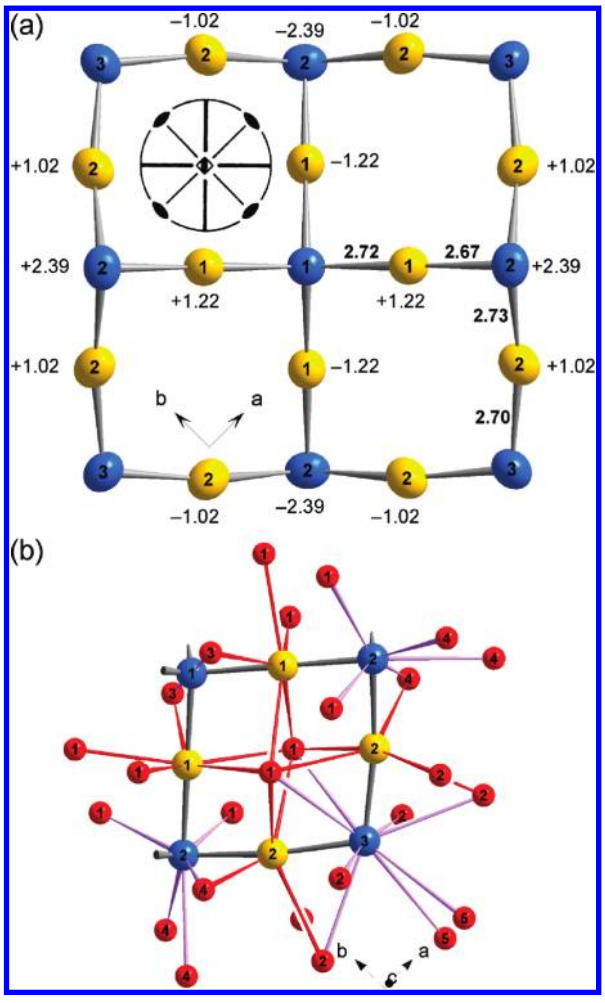

Figure 2. (a) [001] view of the $\{Au_{12}Sn_9\}$ cluster (anisotropic representation of Au (yellow) and Sn (blue) atoms at 90% probability). The labels denote atoms that are located [Å] above (+) and below (−) a plane (00*l*) defined by Sn1 and Sn3 atoms. Inset: Stereograph for point group $\bar{4}2m$ (D_{2d}). (b) The K atoms (red) that are ≤4 Å from an Au or Sn atom and one of the four eight-member rings that build up the cluster are shown.

respect to the large electronegativity differences between K, Au, and Sn (Mulliken values are 2.4, 5.8, and 4.3 eV, respectively[38]), a *Zintl* approach to the electron distribution seems to be reasonable. Thereby, the K atoms are presumed to donate all their valence electrons onto the Au/Sn substructure, which leads to $(K^+)_{23}\{Au_{12}Sn_9\}^{23-}$ and 71 valence electrons (omitting Au $5d^{10}$) that have to be distributed among Au and Sn. The Sn atoms require 12 electrons in total, $4 \times (2b\text{-}Sn3^{2-}) + 4 \times (3b\text{-}Sn2^{-}) + 1 \times (4b\text{-}Sn1^{0})$, and treating each of the 12 2*b*-Au atoms as Au^- leads to $\{Au_{12}Sn_9\}^{24-}$ for a closed shell description. (Assuming Au^+ cations and Sn^{4-} anions would be a much more extreme formulation.) The observed one electron deficiency, which presumably arises for packing reasons, is intriguing for such an open and covalent system; therefore, electronic structure calculations were also done. (No voids or solvent accessible space in the structure could be found with the Calc Void routine implemented in PLATON[39]).

(38) Pearson, R. G. *Inorg. Chem.* **1988**, *27*, 734.
(39) (a) Spek, A. L. *J. Appl. Crystallogr.* **2003**, *36*, 7. (b) *PLATON, A Multipurpose Crystallographic Tool*; Utrecht University: The Netherlands, 2008.

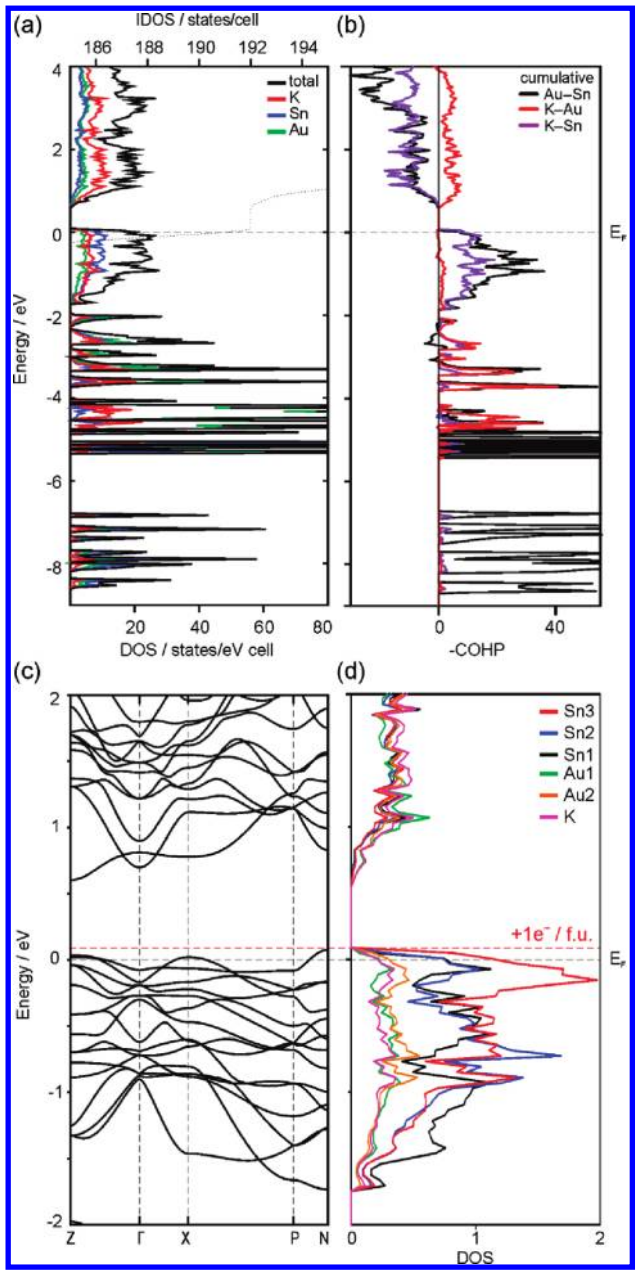

Figure 3. Results of LMTO calculations: (a) Total DOS of the constituent elements. (b) Cumulative COHP, per unit cell (<4 Å). (c) Band dispersion and (d) DOS of Au1−2, Sn1−3, and K (per atom basis) at $E_F \pm 2$ eV.

From LMTO calculations we obtained the "spiky" DOS in Figure 3, which reflects the molecular nature of the compound with low dispersions of the valence orbitals. The Fermi level cuts the DOS on the upper flank of the valence band, leaving an open band and a band gap of ~0.5 eV, the latter arising principally from the pseudo closed-shell Zintl condition. This metallic feature is consistent with the measured magnetic susceptibility, which shows nearly temperature-independent paramagnetic behavior from 50−300 K at 1 T, Supporting Information, Figure S7. Individual DOS diagrams and the separate orbital contributions (Supporting Information, Figure S5) show that most of Au 6s/5d states are filled between −8 and −2 eV. The 5d states, Supporting Information, Figure S5, are very sharp and confined mostly

between −5 and −4 eV. Additionally, a small fraction of Au 6p states is present in the valence band. Sn 5s states appear in a low lying group around −7 eV and are well separated from the valence band, which is dominated by Sn 5p. The band dispersion for $E_F = \pm 2$ eV, Figure 3c, shows that two almost flat bands cross E_F between each of the high symmetry points shown, indicating weak interactions in every reciprocal direction. Fat band representations, Supporting Information, Figure S6, show that these bands mainly originate from Sn 5p functions mixed with K 4s/p states. As we have repeatedly observed in similar systems,[19a,40] the small orbital populations of filled K valence orbitals (per atom) can sum up to a considerable amount, leading to substantial perturbations of the simple ionic treatment for $K_{23}Au_{12}Sn_4$ (above) and an appreciable involvement of the cations in the overall bonding. Evaluations of individual DOS (per atom) around E_F, Figure 3d, shows larger contributions from Sn atoms, and especially from the corner Sn3 atoms (red line), in accord with the classical picture of (non bonding) electron lone pairs. Further, the highest changes in the number of one electron states are observed for Sn3 atoms in this region, and the average K contribution (purple line) is on par with that for the Au atoms (green and orange lines).

Interatomic bonding was analyzed with COHP, which allows weighting of the electronic states according to their energies. As shown in Figure 3b and Table 3, the Au−Sn bonding provides the largest fraction to the COHP, both in terms of −ICOHP values per bond and per unit cell. The lone pair nature of the Sn states around −0.25 eV is indicated by the DOS maxima at the falling upper flank in the Au−Sn COHP. The same region shows interactions between Sn and the surrounding K atoms (purple line) that are individually small, but add ∼20% of the total ICOHP once bond multiplicities are considered (Au−Sn: K−Sn: K−Au bonds are 48: 108: 120 per cell). Of note are also the bonding K−Au interactions (red line in Figure 3b), which occur mostly between −4.5 and −2 eV, a region that covers the Au 5d and K 3d bands. However, in contrast to more condensed, alkali-metal-poorer and gold-richer 3D systems such as A_3Au_5Tr,[40] the K−Sn and K−Au −ICOHP percentiles here are substantial and close to 20% each (Table 3), which is in contradiction to the formal and strict separation of the structure into anionic subunits. It should be noted that no antibonding interactions are present in the vicinity of E_F, which could otherwise explain the electron shortage; rather, spatial (and energy) limitations on the accommodation of an additional K atom must be responsible.

EHTB calculations were done because of the pseudo-molecular nature of the {Au−Sn} substructure. These provide a good qualitative view, although the charges are overestimated (K atoms were not input but considered only as electron donors). Molecular orbitals (MOs) were calculated according to a $\{Au_{12}Sn_9\}^{23-}$ molecular unit and resulted in 95 doubly filled levels plus a singly occupied and non degenerate highest occupied molecular orbital (HOMO, MO96, at −8.3 eV). The HOMO−LUMO gap is ∼2.4 eV, and the MOs span an energy

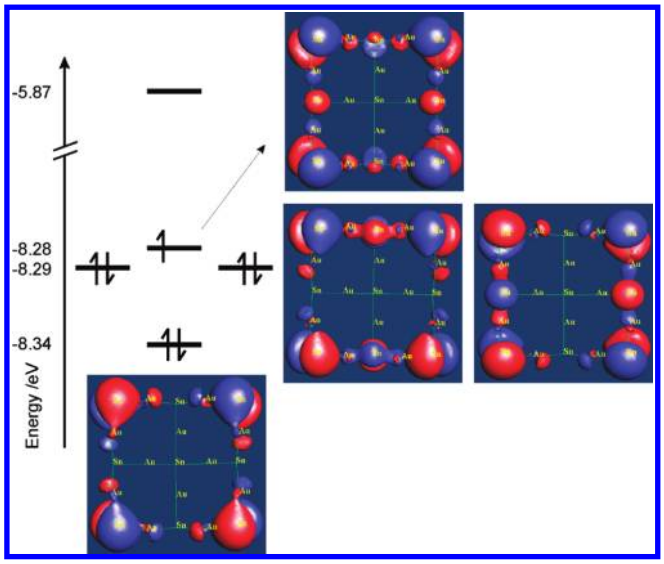

Figure 4. 3D pictures of HOMO-3 to HOMO for the $\{Au_{12}Sn_9\}^{23-}$ cluster as obtained from EHTB calculations.

range from −18.2 to −8.3 eV, which can roughly be divided into three groups: a lowest lying group mainly comprising s−s combinations, a very narrow intermediate group (−15.3 to −15.0 eV) with Au centered MOs displaying nearly noninteracting 5d orbital character, and a valence region with Au s/p−Sn s/p combinations. However, the uppermost frontier orbitals, as shown in Figure 4 for HOMO to HOMO-3, have large $5p_z$ coefficients located at Sn2 and Sn3, indicative of nearly nonbonding orbitals.

Mulliken populations, Table 4, point toward negatively charged Au and Sn atoms, just as approximated by the octet rule, above. Further, the numbers evaluated for different electron counts, 190−192, indicate almost unchanged overlap populations, Table 4, that is, the bonds are optimized in this range. However, notable changes in atom populations can be observed, mostly for the corner Sn3 atoms. These findings are in good agreement with the densities of states obtained from LMTO (above). To access the distinct distribution of Au among the 2*b* sites, the subshell populations of an all-In cluster, $\{In_{12}In_4\}^{23-}$, were evaluated. The more electronegative atoms (here Au) are supposed to prefer the sites with higher populations[36] (although this model effectively omits (relativistic) Au 5d from bonding). The calculated populations 3.99 ("Au1"), 4.07 ("Au2"), 3.54 ("Sn1"), 3.78 ("Sn2"), and 4.71 ("Sn3") agree well with that assumption and the refined crystallographic structure. Certainly, the distinct atom distribution also occurs to maximize the number of strong heteroatomic bonds, as we have observed earlier for $K_{12}Au_{21}Sn_4$.[19a]

Summary and Conclusions

A novel type of $\{Au_{12}Sn_9\}$ cluster found in $K_{23}Au_{12}Sn_9$ represents a rare gold-rich and high nuclearity anion that features a unique arrangement of nearly linear and tetrahedrally coordinated gold and tin atoms, respectively (when lone pairs are included). The coloring scheme follows the general trends for (the more electronegative) gold, that is, preference toward the lower coordinated (or less bonded) positions coupled with a maximization of the number of

(40) Li, B.; Kim, S.-J.; Miller, G. J.; Corbett, J. D. *Inorg. Chem.* **2009**, *48*, 6573.

Table 4. EHTB Overlap and Atom Populations of the $\{Au_{12}Sn_9\}$ Cluster in $K_{23}Au_{12}Sn_9$ evaluated at Different Electron Numbers

	overlap populations			
electrons	Au1−Sn1	Au1−Sn2	Au2−Sn2	Au2−Sn3
190	0.66	0.72	0.66	0.75
191[a]	0.66	0.72	0.66	0.75
192	0.66	0.72	0.66	0.76
	atom populations			
electrons	Au1	Au2	Sn1	Sn2	Sn3
190	11.80	11.84	4.61	5.24	5.63
191[a]	11.80	11.85	4.61	5.27	5.83
192	11.81	11.86	4.61	5.29	6.04

[a] Corresponds to $\{Au_{12}Sn_9\}^{23-}$ in $K_{23}Au_{12}Sn_9$.

heteroatomic bonds. Most intriguingly, the compound deviates from the ideal electron count by minus one electron. LMTO and EHTB band calculations suggest that the electron deficiency naturally lies in states that are least important for the stabilization of the system, that is, in lone pair electrons at 2*b*-Sn atoms, which interact only weakly with the surrounding K atoms. Therefore, the compound forms despite the electronic shortcoming (1 out of 192 electrons!), presumably because of "good" atom packing, rather than in unknown ("worse") alternative structures. Ultimately, the electronic requirements as proposed by *Zintl* rules are also perturbed—considerable participation of K in K− Sn and K−Au bonding has to be included for a comprehensive picture.

Broader variations in the proportions of alkali metal/gold/p element components have revealed other novel and important features regarding bonding and stability. Higher gold contents lead to condensed gold tetrahedral networks, at least in the presence of about one-third as many alkali metal atoms which exhibit important, multiple interactions with and bonding to the gold atoms. This is accompanied by partial segregation of the main-group Tr or *Tt* elements into separate layers or chains and their reduced bonding to gold. In fact, the compositional and structural differences between $K_{12}Au_{21}Sn_4$[19a] and K_3Au_5In (= $K_{12}Au_{20}In_4$)[40] appear to be governed largely by the larger *e*/*a* value in the former. More novel examples certainly must exist.

Acknowledgment. This research was supported by the Office of the Basic Energy Sciences, Materials Sciences Division, U.S. Department of Energy (DOE); Ames Laboratory is operated for DOE by Iowa State University under contract No. DE-AC02-07CH11358.

Supporting Information Available: Single crystal refinement data in CIF format, tables and figures with further crystallographic information. Figures with additional structural details, further LMTO diagrams, and a magnetization plot. This material is available free of charge via the Internet at http://pubs.acs.org.